Received: 5 April 2019 | Revised: 5 July 2019 | Accepted: 26 August 2019

DOI: 10.1002/mrm.27996

NOTE

Magnetic Resonance in Medicine

Venous contribution to sodium MRI in the human brain

Ian D. Driver[1] | **Robert W. Stobbe**[2] | **Richard G. Wise**[1] | **Christian Beaulieu**[2]

[1]Cardiff University Brain Research Imaging Centre, School of Psychology, Cardiff University, Cardiff, United Kingdom

[2]Department of Biomedical Engineering, University of Alberta, Edmonton, Alberta, Canada

Correspondence
Ian D. Driver, Cardiff University Brain Research Imaging Centre, School of Psychology, Cardiff University, Maindy Road, Cardiff CF24 4HQ, United Kingdom.
Email: driveri@cardiff.ac.uk

Funding information
I.D. was supported by the Wellcome Trust ISSF. C.B. is funded by the Canada Research Chairs program and operating support was provided by the Natural Sciences and Engineering Research Council of Canada (NSERC). R.W. acknowledges the support of the Higher Education Funding Council for Wales.

Purpose: Sodium MRI shows great promise as a marker for cerebral metabolic dysfunction in stroke, brain tumor, and neurodegenerative pathologies. However, cerebral blood vessels, whose volume and function are perturbed in these pathologies, have elevated sodium concentrations relative to surrounding tissue. This study aims to assess whether this fluid compartment could bias measurements of tissue sodium using MRI.

Methods: Density-weighted and B_1 corrected sodium MRI of the brain was acquired in 9 healthy participants at 4.7T. Veins were identified using co-registered ^{1}H T_2^*-weighted images and venous partial volume estimates were calculated by downsampling the finer spatial resolution venous maps from the T_2^*-weighted images to the coarser spatial resolution of the sodium data. Linear regressions of venous partial volume estimates and sodium signal were performed for regions of interest including just gray matter, just white matter, and all brain tissue.

Results: Linear regression demonstrated a significant venous sodium contribution above the underlying tissue signal. The apparent venous sodium concentrations derived from regression were 65.8 ± 4.5 mM (all brain tissue), 71.0 ± 7.4 mM (gray matter), and 55.0 ± 4.7 mM (white matter).

Conclusion: Although the partial vein linear regression did not yield the expected sodium concentration in blood (~87 mM), likely the result of point spread function smearing, this regression highlights that blood compartments may bias brain tissue sodium signals across neurological conditions where blood volumes may differ.

KEYWORDS
^{23}Na MRI, blood, sodium MRI, tissue sodium concentration, veins

1 | INTRODUCTION

In the brain, sodium plays a key role in neuronal action potentials, mediates the transport of metabolic substrates through cell membranes and is involved in osmoregulation and pH regulation.[1,2] Sodium (^{23}Na) MRI shows promise as a marker for cerebral metabolic dysfunction in studying stroke,[3-6] brain tumor,[7-11] and neurodegenerative pathologies.[12-17] However, the ^{23}Na MRI signal is greater in cerebrospinal fluid (CSF),[18-21] such that measurements of tissue sodium can be biased by tissue atrophy. Signal contamination from CSF can be corrected prospectively, by suppressing CSF signal using an inversion recovery sequence,[22] or retrospectively, using partial volume correction.[21] Another cerebral fluid compartment,

which has not been considered previously in the context of sodium MRI quantification, is cerebral blood vessels that occupy approximately 5% of the cerebral volume.[23] Human blood sodium concentrations have been measured in vitro by sodium MR spectroscopy as ~87 mM,[24,25] with 2 main constituents of blood being ~60% plasma, an extracellular compartment with ~150 mM sodium concentration, and ~40% red blood cells, an intracellular compartment with ~15 mM sodium concentration.[25] By using a shift reagent in the rat brain, a significant 16% intravascular sodium signal increase was observed with NMR during a hypercapnia-induced increase in cerebral blood volume (CBV).[26]

The space occupied by cerebral blood vessels is perturbed in pathologies, such as brain tumor, stroke and multiple sclerosis. Angiogenesis is a key part of the pathophysiology in cancer,[27] leading to a focal increase in CBV. Stroke, whether it is ischemic or hemorrhagic, has a significant effect on CBV.[28] Multiple sclerosis lesions appear to form around veins,[29,30] so the sodium MRI signals in these lesions will include a significant venous compartment. Therefore, understanding the scale of sodium signal in cerebral blood, relative to tissue, becomes important in interpreting sodium signals when investigating the pathophysiology of these conditions using sodium MRI, where CBV is likely to be perturbed. In this study, the ^{23}Na MRI signal from cerebral veins, which are readily identifiable using T_2^*-weighted MRI[31] was assessed and compared with the ^{23}Na MRI signal from brain tissue.

2 | METHODS

Nine healthy subjects (age 30 ± 6 years, 5 female/4 male) participated in this study. The Health Research Ethics Board at the University of Alberta approved this study and subjects gave written informed consent. MRI data were acquired on a Varian Inova 4.7T whole-body system in 2 contiguous sessions with (i) ^{23}Na MRI data with a single-tuned birdcage head coil and (ii) ^{1}H MRI data with a birdcage transmit head coil and 4-element receive array. Density-weighted whole-brain ^{23}Na images (Figures 1 and 2A) were acquired using twisted projection imaging with 18 ms readout duration and voxels of $3.2 \times 3.2 \times 6.4$ mm^3 (defined by $1/(2k_{max})$). A total of 6000 projections ($\rho = 0.2$) fully sampled k-space with sampling density designed for an approximately Hamming filtering shape to reduce CSF ringing.[32] The parameters of TR = 85 ms, echo time = 0.11 ms, and flip angle = 30° were selected to minimize both T_1 and rapid biexponential T_2 weighting as well as signal loss from residual quadrupole splitting.[33] The acquisition of 1 average yielded a scan time of 8.5 min. B_1 maps were acquired from 2 low resolution images using a double flip-angle approach and used to correct the density weighted signal variation as a result of flip angle (B_1^+) and receive sensitivity (B_1^-). Anatomical ^{1}H MPRAGE (whole-brain, 1 mm isotropic, repetition time = 1650 ms, inversion time = 725 ms, echo time = 4.5 ms, flip angle 10°) and FLASH (50 axial slices, $0.5 \times 0.5 \times 2$ mm^3, repetition time = 1540 ms, echo time = 15 ms) were acquired for segmentation of tissue and veins, respectively.

N4 bias field correction[34] was performed on the MPRAGE and FLASH images before segmentation. Tissue segmentation was performed on the MPRAGE using the FSL Brain Extraction Tool (BET) and FMRIB's Automated Segmentation Tool (FSL 5.0.9, fMRIB, Oxford, UK). This resulted in gray matter (GM), white matter (WM), and CSF partial volume estimate (PVE) maps. Segmentation of veins was performed on the FLASH images, because cerebral veins are hypo-intense on these T_2^*-weighted images. To minimize image contrast other than signal decrease over the small spatial scales associated with veins, a 3 mm full-width-half-maximum Gaussian high-pass spatial filter was applied to the FLASH images. A brain mask (performed using BET) eroded by 3 voxels (7×7 kernel) was then applied to remove filter artifacts at the edge of the brain. The hypo-intense veins on the T_2^* images are manifest with negative values on the high-pass filtered images, while brain tissue retains an average contrast near zero apart from small positive/negative variation at tissue boundaries. A minimum negative threshold was selected to create a binary vein mask, while ensuring that negative high-pass values resulting from tissue boundaries did not contribute to the mask (example shown in Figure 2). When the $0.5 \times 0.5 \times 2$ mm^3 binary vein masks are resampled to the $3.2 \times 3.2 \times 6.4$ mm^3 voxel size of the ^{23}Na images (see below), these masks become vein PVE maps with 131 FLASH voxels for each ^{23}Na voxel.

For the purposes of subsequent analysis, ^{23}Na images were reconstructed onto an $88 \times 88 \times 44$ grid ($3.2 \times 3.2 \times 6.4$ mm^3). However, solely to assist with registration from the MPRAGE and FLASH images to ^{23}Na space, an additional $616 \times 616 \times 308$ reconstruction was also performed, using zero filling. The finer spatial resolution of this reference provided improved registration accuracy, compared with co-registering the MPRAGE and FLASH directly to the low-resolution ^{23}Na image. Rigid-body registration was performed using FMRIB's Linear Image Registration Tool (FSL, FMRIB, Oxford, UK) to realign MPRAGE and FLASH images to the zero-filled ^{23}Na image. These registrations were applied to the tissue segmentation maps. The zero-filled $616 \times 616 \times 308$ grid maps directly onto the low-resolution $88 \times 88 \times 44$ grid through a set of $7 \times 7 \times 7$ sub-voxels within each single voxel of the low-resolution grid. Therefore, the tissue segmentation maps were down-sampled from the $616 \times 616 \times 308$ matrix to the $88 \times 88 \times 44$ matrix by taking the mean of each $7 \times 7 \times 7$ block of sub-voxels. This form of downsampling does not cause any additional spatial smoothing (over that arising from the image registration), as no interpolation is required. Note that the FLASH dataset did not cover the

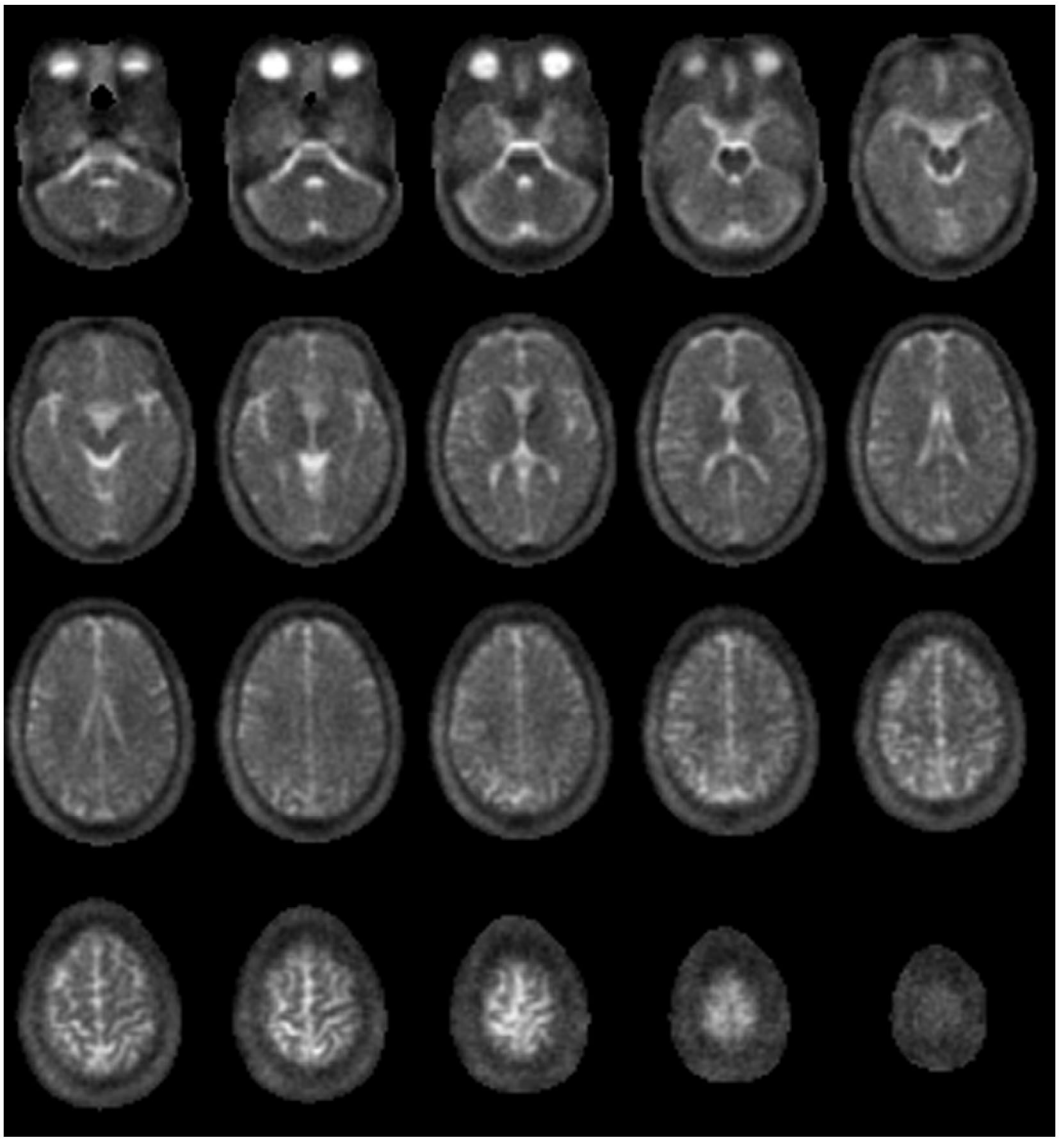

FIGURE 1 Twenty axial slices of ^{23}Na, showing the central portion of the data, from a healthy 30-year-old male volunteer

most inferior portion of the brain (see Figure 2 for extent), resulting in areas where no venous information was available. Therefore, these regions were excluded from subsequent sodium analysis.

No external references were acquired for calibrating sodium concentration, so signal from vitreous humor (VH) was used as a reference for sodium signals from other tissues. VH volumes in the eyeballs were sufficiently large to provide a central sodium signal free from partial volume bias. A literature value of $[Na]_{VH} = 134$ mM[20] was assumed, while the density weighted acquisition parameters mitigated against differences in tissue relaxation values.[33] A VH region of interest (ROI) was drawn manually on the MPRAGE, then realigned and downsampled to the ^{23}Na image. This VH ROI was eroded using a $3 \times 3 \times 3$ cubic voxel structure element and VH sodium signal was measured as the mean across this eroded ROI.

A brain tissue mask was created by excluding any voxels with CSF PVE ≥ 0.01. This was necessary to minimize contamination from the relatively high sodium concentration in CSF (~150 mM). Note that larger veins are typically found at the cortical surface and so generally lay adjacent to CSF spaces. The conservative CSF masking procedure eliminates these voxels from analysis. The result of CSF exclusion can be observed by comparing the vein PVE map (Figure 3B) with the CSF excluded vein PVE map (Figure 3D). Within the brain tissue mask, brain tissue was segmented into GM and WM ROIs using a 0.5 PVE threshold. However, the segmentation of the 4.7T MPRAGE images did not perform well in regions of the thalamus and putamen, erroneously classifying parts as WM. These regions were identified manually and excluded from the WM ROIs to ensure proper tissue classification. As a result, these regions were not part of either the WM or GM ROIs; however, they remain within the full brain

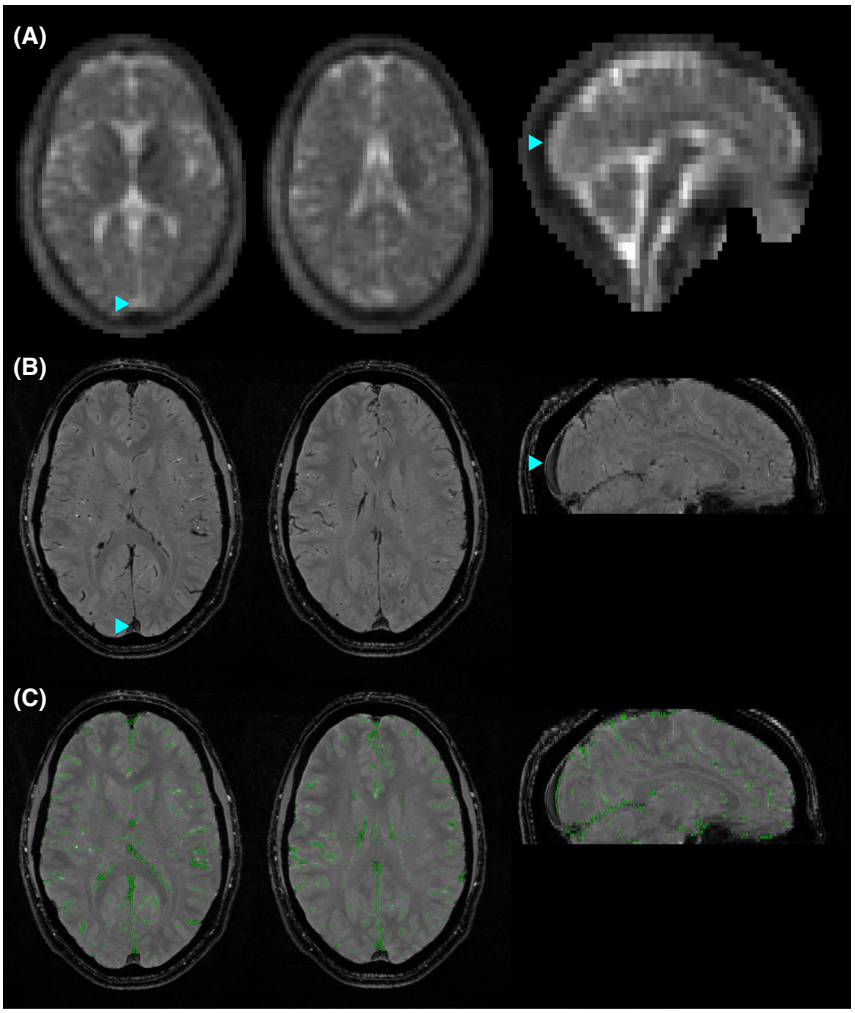

FIGURE 2 Sodium signal in the superior sagittal sinus (SSS), a major vein, and demonstration of vein masking. A, Two axial slices and 1 sagittal slice of an example density-weighted ^{23}Na dataset, demonstrating higher sodium signal in the SSS (blue arrowhead) than the surrounding tissue. B, ^{1}H FLASH image with veins appearing hypointense. Blue arrowheads mark the same point on the SSS as shown in (A). C, Demonstrating the binary vein mask (green) overlaid on the ^{1}H FLASH image from which the mask is calculated. Note that the SSS is not included in the mask as its diameter is larger than the 3 mm spatial filter. The images are from a healthy 30-year-old male volunteer

tissue mask. Representative GM and WM ROIs are shown in Figure 3E.

To determine the effect of elevated sodium concentration within blood on tissue sodium concentration measurements, a linear regression was performed between vein PVE and ^{23}Na signal (relative to VH signal) over every voxel within the brain tissue mask. This regression was then redone for voxels only within the WM ROIs and only in the GM ROIs. For each volunteer, this spatial regression yielded ^{23}Na blood values (relative to VH) calculated at vein PVE = 1. Note that the superior sagittal sinus (SSS) was not included in the vein PVE map, as it was too large to be resolved by the high-pass spatial filter during vein segmentation. Alternatively, an ROI including the SSS was drawn manually on the ^{1}H FLASH image, and resampled into ^{23}Na space creating a SSS PVE map. Average signal was calculated across SSS PVE $\geq$ 0.5 voxels. These values (converted to concentration according to $[Na]_{VH}$ = 134 mM)[20] were then compared with tissue sodium values (similarly converted to concentration) directly measured from the WM and GM ROIs, and with blood concentration from the literature. All values were reported as mean $\pm$ SEM across 9 subjects. Venous signals were compared with mean tissue signal over the ROI they were calculated from using a Bonferroni-corrected paired 2-tailed *t*-test. SSS signal was compared with GM tissue signal.

3 | RESULTS

An example of density-weighted ^{23}Na images is shown for the whole brain in Figure 1. Higher sodium signals in veins is most noticeable in the major draining vein of the brain, the SSS (Figure 2A), which is visible in ^{23}Na images from all subjects. Veins mapped on the ^{1}H FLASH T_2^*-weighted images occupied 3.1 $\pm$ 0.2% of the whole brain volume (mean $\pm$ SEM across 9 subjects). The maximum vein PVE within the brain tissue mask ranged from 20-57% of the voxel (median 36%).

All vein sodium signal calculations were significantly greater than the mean tissue signal of the ROI they were calculated from, as follows: Vein PVE regression over all voxels within the brain tissue mask yielded a venous sodium signal 49 $\pm$ 3% of VH signal, or a VH normalized

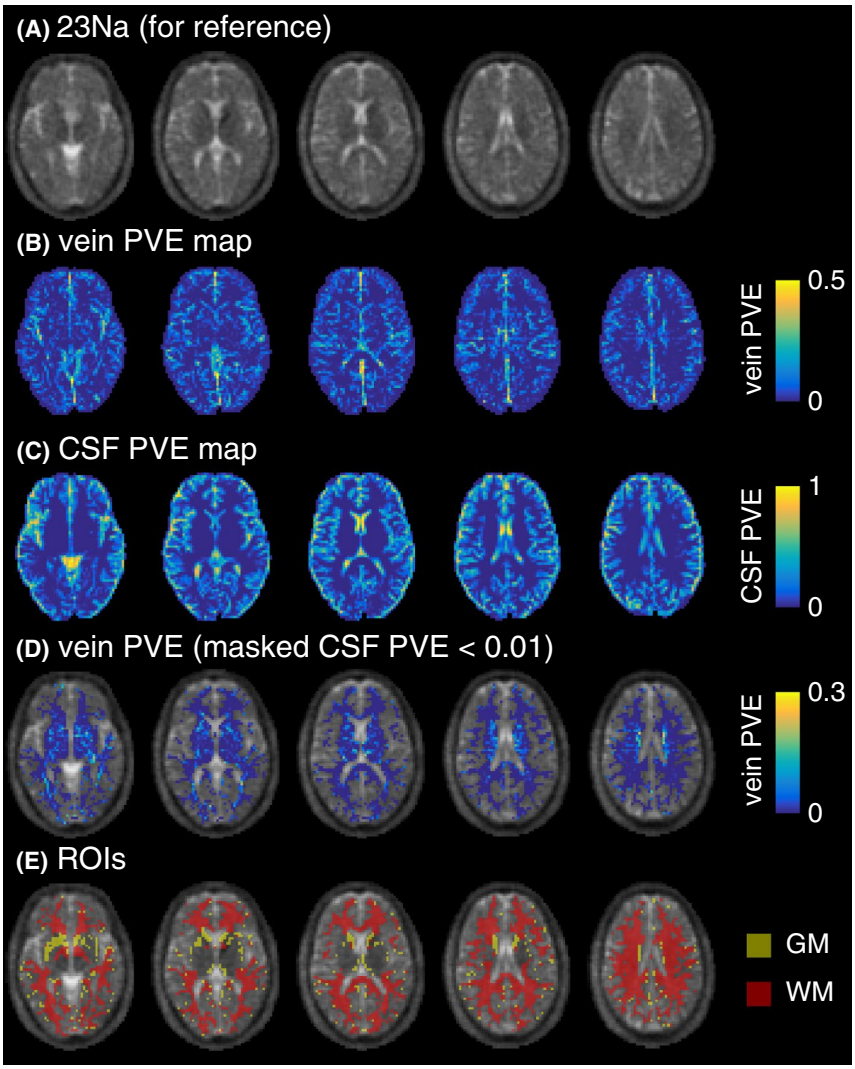

FIGURE 3 Illustration of partial volume estimate (PVE) maps shown in 5 axial slices from a healthy 30-year-old male volunteer. A, ^{23}Na image, for reference. B, Vein PVE map. C, CSF PVE map, showing some spatial overlap with vein PVE (N.B. scale not matching (B), optimized for data range). D, Vein PVE map masked by CSF PVE < 0.01, showing the full brain tissue mask used to calculate venous sodium signal (N.B. scale not matching (B, C), optimized for data range). E, Example GM and WM ROIs

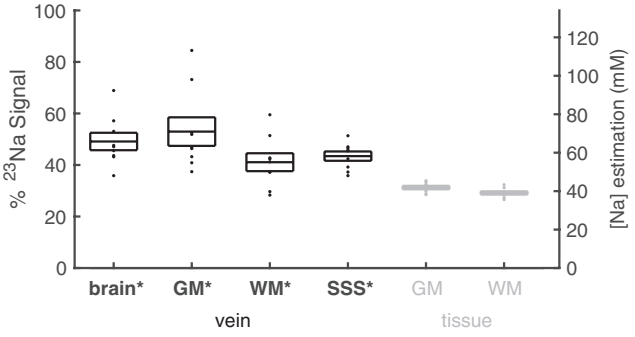

FIGURE 4 Sodium signals as a percentage of VH sodium signals. Vein sodium signals determined from regression over whole brain tissue, GM, and WM regions and averaged over the SSS are shown in black. Tissue sodium signals from GM and WM are shown in gray. The right-hand axis shows estimated sodium concentrations, based on a literature value of 134 mM[20] for VH. Boxes show mean ± SEM across 9 subjects, and dots show each individual subject's value. *$P < 0.05$ compared with tissue signal for each region and to GM for the SSS (Bonferroni-corrected paired *t*-test)

apparent concentration value of 65.8 ± 4.5 mM (**$t(8) = 6.3$; $P = 9 \times 10^{-4}$**). Regression in GM ROIs yielded apparent venous concentration of 71.0 ± 7.4 mM (**$t(8) = 4.3$; $P = 0.01$**), while regression in WM ROIs yielded apparent venous concentration of 55.0 ± 4.7 mM (**$t(8) = 3.5$; $P = 0.03$**). SSS venous concentration was measured as 58.2 ± 2.4 (**$t(8) = 10.6$; $P = 2 \times 10^{-5}$**). The apparent tissue sodium concentration values measured in the WM and GM ROIs were 39.1 ± 0.8 mM and 41.9 ± 0.9 mM, respectively. Figure 4 presents individual subject data for all measurements.

4 | DISCUSSION

The regression between vein PVEs and density-weighted sodium signal yielded average (over all volunteers) apparent sodium concentration in veins of 55 mM-71 mM (depending on which brain tissue voxels were included in the regression). This is considerably less than the ~87 mM previously

measured in vitro for human blood.[24,25] However, the result that regression produced significantly greater vein concentration values for all brain tissue (69 ± 11%), GM (69 ± 16%), and WM (42 ± 13%) demonstrates that vein partial volume does contribute to the sodium signal within brain voxels. Although this contribution may not be directly visible on a ^{23}Na MRI image, it is sufficient to produce the positive correlations measured in this study.

The apparent sodium concentrations reported were calculated by comparing (B_1 corrected and density-weighted) sodium signal measurements and regression values with that in VH. Using VH = 134 mM,[20] apparent sodium concentration values of 39.1 ± 0.8 and 41.9 ± 0.9 mM were measured in WM and GM, respectively. These are at the midpoint of existing literature values.[13,15-17,19-21,35-37] Although the apparent sodium concentration values reported in this study are sensitive to inter-subject sodium VH concentration variability, the variance in WM and GM measurements is small across subjects. This can be seen in the standard deviation values reported above and in Figure 4. Although this method of apparent sodium concentration measurement is also sensitive to the accuracy of the VH concentration value from the literature, absolute concentration values are not necessary to demonstrate through regression that sodium signal from veins contributes to brain tissue voxels.

The density-weighted ^{23}Na MRI images have insufficient spatial resolution to directly measure blood sodium signal in any of the intracranial veins, including the SSS. The twisted projection acquisition scheme used for the ^{23}Na sequences has a point spread function (PSF) full-width-half-maximum of 7.1 mm in-plane (and double that out-of-plane). This is calculated for the T_{2fast} = 2 ms and T_{2slow} = 17 ms of blood[38,39] and includes the Hamming-like filter for Gibbs ringing removal. As a result, the elevated ^{23}Na signal originating from veins will be smeared according to the PSF of the sodium images.[40] Signal originating from a vein will contribute only part of its signal to the voxel in which it resides, the rest will contribute to the surrounding voxels. This PSF smearing (at least partially) explains why the apparent blood sodium concentrations measured from all regression experiments are lower than that expected from previous in vitro study.[24,25] In addition, the spatial extent of veins will be overestimated due to intra-voxel dephasing of adjacent tissue signal, a result of the vein's fringe field. Thus, the vein PVE maps will overestimate the relative contribution of a small vein to the sodium dataset, resulting in the regression of smaller blood sodium concentration values.

The vein PVE–sodium regression including voxels in just WM ROIs yielded smaller apparent blood sodium concentration values than the regressions including voxels in GM. This is likely because the WM ROIs contain primarily small veins. The additional signal contribution to a voxel from small veins will in turn be small, yielding an effect more sensitive to noise. GM contains a greater number of larger veins with greater signal increase.

To assess the contribution of blood to tissue sodium signals, literature values for CBV of 2.7% for WM[41-43] and 5% for GM[23,42,43] were assumed, and the sodium signal from all blood vessels was assumed equal to that directly measured in the literature (~87 mM). Correcting for the blood signal using these values reduced the tissue sodium concentration values by 3.4% and 5.7% for WM and GM, respectively. Total sodium concentrations were simulated for a range of CBV values from 0 to 30% (approximate intra-subject range of vein PVE) in Figure 5. Although the values measured in this study were smeared by the PSF, the full blood vessel signal contribution is still contained within the measured tissue sodium signal, spread across a greater number of pixels.

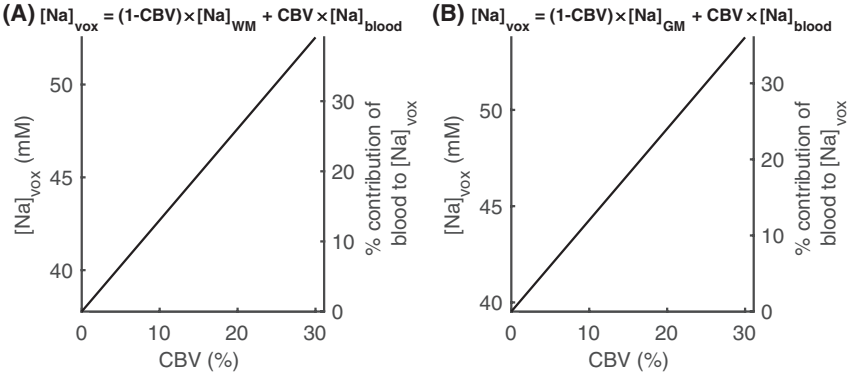

FIGURE 5 Simulation of the signal contribution from blood to WM (A) and GM (B) tissue sodium concentration measurements. $[Na]_{vox}$ is the sodium concentration that would be measured for $[Na]_{WM/GM}$ containing a CBV with sodium concentration $[Na]_{blood}$ = 87 mM.[24,25] $[Na]_{WM}$ = 37.8 mM is the WM sodium concentration with the blood contribution removed, calculated based on the measured $[Na]_{WM}$ = 39.1 mM corrected for CBV = 2.7%.[41-43] $[Na]_{GM}$ = 39.5 mM is the GM sodium concentration with the blood contribution removed, calculated based on the measured $[Na]_{GM}$ = 41.9 mM corrected for CBV = 5%.[23,42,43] The right-hand axes show the contribution of blood to the total sodium signal. The CBV range of 0 to 30% reflects the typical intra-subject range of values across voxels in the vein PVE map within the region used to calculate venous sodium signal

While this study focuses on cerebral veins (which are visible on the T_2^*-weighted ^{1}H images), the partial volume contribution of arteries is also expected to increase tissue sodium concentration (and likely affected the regression performed in this study). Because the plasma volume fraction is similar in arteries and veins,[44] these blood vessels should contain similar sodium concentrations. However, the plasma volume fraction is ~25% higher in microvasculature.[23,45] With plasma sodium concentration on the order of 150 mM,[25] microvasculature is likely to have a greater sodium concentration than veins and arteries.

The distinct sodium MRI characteristics of blood have significance for studies where the pathophysiology includes cerebral blood vessels, such as brain tumor,[7-11] stroke,[3-6] and multiple sclerosis.[13,15-17] There can be significant focal increases in the size of the blood volume compartment in these pathologies. These results are also of significance for recent studies demonstrating sodium fMRI contrast,[46,47] where functional responses of interest will be accompanied by focal vasodilation. For example, focal arterial blood volume can increase in the range of 30-60% in response to a functional stimulus.[48-52] The apparent tissue sodium signal increase due to an increase in volume of blood vessels could be misattributed to a neuronal mechanism, if not accounted for. Studies of tissue sodium concentration in conditions such as above, where cerebral blood vessels have a significant role, could also assess CBV[41-43,53] to control for the blood volume contribution to the sodium signal.

5 | CONCLUSIONS

It was demonstrated that tissue sodium concentration increases in proportion to the partial vein contribution to a voxel. Thus, tissue sodium concentrations may be overestimated in the presence of large blood vessels, and may vary as a result of blood vessel and blood flow perturbation.

ACKNOWLEDGMENT

The authors thank Peter Seres for his assistance with image analysis.

ORCID

Ian D. Driver https://orcid.org/0000-0001-6815-0134
Robert W. Stobbe https://orcid.org/0000-0002-6223-5222

REFERENCES

1. Madelin G, Regatte RR. Biomedical applications of sodium MRI in vivo. *J Magn Reson Imaging*. 2013;38:511–529.
2. Thulborn KR. Quantitative sodium MR imaging: a review of its evolving role in medicine. *NeuroImage*. 2018;168:250–268.
3. Thulborn KR, Davis D, Snyder J, Yonas H, Kassam A. Sodium MR imaging of acute and subacute stroke for assessment of tissue viability. *Neuroimaging Clin N Am*. 2005;15(639–653):xi–xii.
4. Hussain MS, Stobbe RW, Bhagat YA, et al. Sodium imaging intensity increases with time after human ischemic stroke. *Ann Neurol*. 2009;66:55–62.
5. Tsang A, Stobbe RW, Asdaghi N, et al. Relationship between sodium intensity and perfusion deficits in acute ischemic stroke. *J Magn Reson Imaging*. 2011;33:41–47.
6. Boada FE, Qian Y, Nemoto E, et al. Sodium MRI and the assessment of irreversible tissue damage during hyper-acute stroke. *Transl Stroke Res*. 2012;3:236–245.
7. Ouwerkerk R, Bleich KB, Gillen JS, Pomper MG, Bottomley PA. Tissue sodium concentration in human brain tumors as measured with 23Na MR imaging. *Radiology*. 2003;227:529–537.
8. Thulborn KR, Lu A, Atkinson IC, Damen F, Villano JL. Quantitative sodium MR imaging and sodium bioscales for the management of brain tumors. *Neuroimaging Clin N Am*. 2009;19:615–624.
9. Nagel AM, Bock M, Hartmann C, et al. The potential of relaxation-weighted sodium magnetic resonance imaging as demonstrated on brain tumors. *Invest Radiol*. 2011;46:539–547.
10. Fiege DP, Romanzetti S, Mirkes CC, Brenner D, Shah NJ. Simultaneous single-quantum and triple-quantum-filtered MRI of 23Na (SISTINA). *Magn Reson Med*. 2013;69:1691–1696.
11. Biller A, Badde S, Nagel A, et al. Improved brain tumor classification by sodium MR imaging: prediction of IDH mutation status and tumor progression. *AJNR Am J Neuroradiol*. 2016;37:66–73.
12. Mellon EA, Pilkinton DT, Clark CM, et al. Sodium MR imaging detection of mild Alzheimer disease: preliminary study. *AJNR Am J Neuroradiol*. 2009;30:978–984.
13. Inglese M, Madelin G, Oesingmann N, et al. Brain tissue sodium concentration in multiple sclerosis: a sodium imaging study at 3 Tesla. *Brain*. 2010;133(Pt 3):847–857.
14. Reetz K, Romanzetti S, Dogan I, et al. Increased brain tissue sodium concentration in Huntington's Disease - a sodium imaging study at 4 T. *NeuroImage*. 2012;63:517–524.
15. Zaaraoui W, Konstandin S, Audoin B, et al. Distribution of brain sodium accumulation correlates with disability in multiple sclerosis: a cross-sectional 23Na MR imaging study. *Radiology*. 2012;264:859–867.
16. Paling D, Solanky BS, Riemer F, et al. Sodium accumulation is associated with disability and a progressive course in multiple sclerosis. *Brain*. 2013;136(Pt 7):2305–2317.
17. Maarouf A, Audoin B, Konstandin S, et al. Topography of brain sodium accumulation in progressive multiple sclerosis. *MAGMA*. 2014;27:53–62.
18. Harrington MG, Salomon RM, Pogoda JM, et al. Cerebrospinal fluid sodium rhythms. *Cerebrospinal Fluid Res*. 2010;7:3.
19. Atkinson IC, Lu A, Thulborn KR. Clinically constrained optimization of flexTPI acquisition parameters for the tissue sodium concentration bioscale. *Magn Reson Med*. 2011;66:1089–1099.
20. Mirkes CC, Hoffmann J, Shajan G, Pohmann R, Scheffler K. High-resolution quantitative sodium imaging at 9.4 Tesla. *Magn Reson Med*. 2015;73:342–351.
21. Niesporek SC, Hoffmann SH, Berger MC, et al. Partial volume correction for in vivo (23)Na-MRI data of the human brain. *NeuroImage*. 2015;112:353–363.

22. Stobbe R, Beaulieu C. In vivo sodium magnetic resonance imaging of the human brain using soft inversion recovery fluid attenuation. *Magn Reson Med*. 2005;54:1305–1310.
23. Griffeth VE, Buxton RB. A theoretical framework for estimating cerebral oxygen metabolism changes using the calibrated-BOLD method: modeling the effects of blood volume distribution, hematocrit, oxygen extraction fraction, and tissue signal properties on the BOLD signal. *NeuroImage*. 2011;58:198–212.
24. Bottomley PA. Sodium MRI in human heart: a review. *NMR Biomed*. 2016;29:187–196.
25. Pettegrew JW, Woessner DE, Minshew NJ, Glonek T. Sodium-23 NMR analysis of human whole blood, erythrocytes, and plasma. Chemical shift, spin relaxation, and intracellular sodium concentration studies. *J Magn Reson*. 1969;1984(57):185–196.
26. Ronen I, Kim SG. Measurement of intravascular Na(+) during increased CBF using (23)Na NMR with a shift reagent. *NMR Biomed*. 2001;14:448–452.
27. Bergers G, Benjamin LE. Tumorigenesis and the angiogenic switch. *Nat Rev Cancer*. 2003;3:401–410.
28. Donnan GA, Fisher M, Macleod M, Davis SM. Stroke. *Lancet*. 2008;371:1612–1623.
29. Samaraweera APR, Clarke MA, Whitehead A, et al. The central vein sign in multiple sclerosis lesions is present irrespective of the T2* sequence at 3 T. *J Neuroimaging*. 2017;27:114–121.
30. Tallantyre EC, Brookes MJ, Dixon JE, Morgan PS, Evangelou N, Morris PG. Demonstrating the perivascular distribution of MS lesions in vivo with 7-Tesla MRI. *Neurology*. 2008;70:2076–2078.
31. Reichenbach JR, Venkatesan R, Schillinger DJ, Kido DK, Haacke EM. Small vessels in the human brain: MR venography with deoxyhemoglobin as an intrinsic contrast agent. *Radiology*. 1997;204:272–277.
32. Stobbe R, Beaulieu C. Advantage of sampling density weighted apodization over postacquisition filtering apodization for sodium MRI of the human brain. *Magn Reson Med*. 2008;60:981–986.
33. Stobbe RW, Beaulieu C. Residual quadrupole interaction in brain and its effect on quantitative sodium imaging. *NMR Biomed*. 2016;29:119–128.
34. Tustison NJ, Avants BB, Cook PA, et al. N4ITK: improved N3 bias correction. *IEEE Trans Med Imaging*. 2010;29:1310–1320.
35. Lu A, Atkinson IC, Claiborne TC, Damen FC, Thulborn KR. Quantitative sodium imaging with a flexible twisted projection pulse sequence. *Magn Reson Med*. 2010;63:1583–1593.
36. Qian Y, Zhao T, Zheng H, Weimer J, Boada FE. High-resolution sodium imaging of human brain at 7 T. *Magn Reson Med*. 2012;68:227–233.
37. Ridley B, Nagel AM, Bydder M, et al. Distribution of brain sodium long and short relaxation times and concentrations: a multi-echo ultra-high field (23)Na MRI study. *Sci Rep*. 2018;8:4357.
38. Constantinides CD, Gillen JS, Boada FE, Pomper MG, Bottomley PA. Human skeletal muscle: sodium MR imaging and quantification-potential applications in exercise and disease. *Radiology*. 2000;216:559–568.
39. Madelin G, Jerschow A, Regatte RR. Sodium relaxation times in the knee joint in vivo at 7T. *NMR Biomed*. 2012;25:530–537.
40. Stobbe RW, Beaulieu C. Calculating potential error in sodium MRI with respect to the analysis of small objects. *Magn Reson Med*. 2018;79:2968–2977.
41. Doucette J, Wei L, Hernández-Torres E, et al. Rapid solution of the Bloch-Torrey equation in anisotropic tissue: application to dynamic susceptibility contrast MRI of cerebral white matter. *NeuroImage*. 2019;185:198–207.
42. Leenders KL, Perani D, Lammertsma AA, et al. Cerebral blood flow, blood volume and oxygen utilization. Normal values and effect of age. *Brain*. 1990;113(Pt 1):27–47.
43. Liu D, Xu F, Lin DD, van Zijl P, Qin Q. Quantitative measurement of cerebral blood volume using velocity-selective pulse trains. *Magn Reson Med*. 2017;77:92–101.
44. Yang ZW, Yang SH, Chen L, Qu J, Zhu J, Tang Z. Comparison of blood counts in venous, fingertip and arterial blood and their measurement variation. *Clin Lab Haematol*. 2001;23:155–159.
45. Sakai F, Nakazawa K, Tazaki Y, et al. Regional cerebral blood volume and hematocrit measured in normal human volunteers by single-photon emission computed tomography. *J Cereb Blood Flow Metab*. 1985;5:207–213.
46. Bydder M, Zaaraoui W, Ridley B, et al. Dynamic (23)Na MRI - A non-invasive window on neuroglial-vascular mechanisms underlying brain function. *NeuroImage*. 2019;184:771–780.
47. Gandini Wheeler-Kingshott CAM, Riemer F, Palesi F, et al. Challenges and perspectives of quantitative functional sodium imaging (fNaI). *Front Neurosci*. 2018;12:810.
48. Brookes MJ, Morris PG, Gowland PA, Francis ST. Noninvasive measurement of arterial cerebral blood volume using Look-Locker EPI and arterial spin labeling. *Magn Reson Med*. 2007;58:41–54.
49. Kim T, Hendrich KS, Masamoto K, Kim SG. Arterial versus total blood volume changes during neural activity-induced cerebral blood flow change: implication for BOLD fMRI. *J Cereb Blood Flow Metab*. 2007;27:1235–1247.
50. Ho YC, Petersen ET, Zimine I, Golay X. Similarities and differences in arterial responses to hypercapnia and visual stimulation. *J Cereb Blood Flow Metab*. 2011;31:560–571.
51. Hua J, Qin Q, Donahue MJ, Zhou J, Pekar JJ, van Zijl PC. Inflow-based vascular-space-occupancy (iVASO) MRI. *Magn Reson Med*. 2011;66:40–56.
52. Jahanian H, Peltier S, Noll DC, Hernandez GL. Arterial cerebral blood volume-weighted functional MRI using pseudo-continuous arterial spin tagging (AVAST). *Magn Reson Med*. 2015;73:1053–1064.
53. Lu H, Golay X, Pekar JJ, Van Zijl PC. Functional magnetic resonance imaging based on changes in vascular space occupancy. *Magn Reson Med*. 2003;50:263–274.

How to cite this article: Driver ID, Stobbe RW, Wise RG, Beaulieu C. Venous contribution to sodium MRI in the human brain. *Magn Reson Med*. 2020;83:1331–1338. https://doi.org/10.1002/mrm.27996